Exciton-Exciton Annihilation Is Coherently Suppressed in H-Aggregates, but Not in J-Aggregates

Tempelaar, Roel; Jansen, Thomas L. C.; Knoester, Jasper

Published in:
The Journal of Physical Chemistry Letters

DOI:
10.1021/acs.jpclett.7b02745

Publication date:
2017

THE JOURNAL OF PHYSICAL CHEMISTRY Letters

Letter

Cite This: J. Phys. Chem. Lett. 2017, 8, 6113−6117

pubs.acs.org/JPCL

Exciton−Exciton Annihilation Is Coherently Suppressed in H-Aggregates, but Not in J-Aggregates

Roel Tempelaar,*[,†,‡] Thomas L. C. Jansen,[†] and Jasper Knoester*[,†]

[†]Zernike Institute for Advanced Materials, University of Groningen, Nijenborgh 4, 9747 AG Groningen, The Netherlands

[‡]Department of Chemistry, Columbia University, 3000 Broadway, New York, New York 10027, United States

Supporting Information

ABSTRACT: We theoretically demonstrate a strong dependence of the annihilation rate between (singlet) excitons on the *sign* of dipole−dipole couplings between molecules. For molecular H-aggregates, where this sign is positive, the phase relation of the delocalized two-exciton wave functions causes a destructive interference in the annihilation probability. For J-aggregates, where this sign is negative, the interference is constructive instead; as a result, no such coherent suppression of the annihilation rate occurs. As a consequence, room temperature annihilation rates of typical H- and J-aggregates differ by a factor of ∼3, while an order of magnitude difference is found for low-temperature aggregates with a low degree of disorder. These findings, which explain experimental observations, reveal a fundamental principle underlying exciton−exciton annihilation, with major implications for technological devices and experimental studies involving high excitation densities.

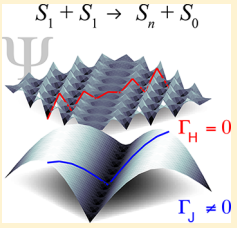

The annihilation between (singlet) excitons is a dominant contributor to the optoelectronic properties of materials at high excitation densities. It is considered a major loss mechanism in lasers based on organic thin films[1] and polariton microcavities,[2] as well as organic light-emitting diodes.[3] It is also an important factor impacting the excited state dynamics of single-walled carbon nanotubes[4−6] and inorganic monolayers.[7] At the same time, it has a functional purpose in the formation of interchain species[8] and separated charges[9,10] in organic electronics. Exciton−exciton annihilation occurring in nonlinear spectroscopy at high fluences can complicate the interpretation of the measurements,[11−13] while it also serves as a means to study the structure and functioning of materials.[14,15] In particular, it continues to find widespread application to determine exciton diffusion lengths through its imprints on laser fluence-dependent time-resolved spectroscopic measurements.[16−21]

Exciton−exciton annihilation (EEA) is commonly regarded as an incoherent, stochastic process, being described by the bimolecular rate equation

$$\Gamma = \alpha n^2 \tag{1}$$

with Γ as the annihilation rate, n as the exciton density, and α as a proportionality constant. A few theoretical studies[22−26] have considered EEA beyond such a macroscopic description, and investigated the role of microscopic properties such as exciton coherence length[22,23] and relaxation pathways.[24] Nevertheless, our microscopic understanding of EEA remains limited, which hampers the rational design of materials with desirable EEA qualities. In particular, experiments have shown EEA to be much more effective in J-aggregates than in H-aggregates,[27−31] for which a convincing explanation remains to be found.

Here, by applying a microscopic model, we demonstrate a dramatic dependence of EEA on the *sign* of dipole−dipole couplings between molecules, J, which drives exciton delocalization. For H-aggregates, where $J > 0$, the phase relation of the thermally populated, delocalized two-exciton wave functions contributes destructively to Γ. By contrast, no such destructive interference occurs for J-aggregates, for which $J < 0$.

Figure 1 provides a microscopic representation of EEA. Excitation energy is transferred resonantly between two nearby molecules in their S_1 excited state, lowering one molecule to the ground state (S_0) while promoting the other to a higher-lying singlet state (S_n), upon which phonon-assisted relaxation of S_n occurs. If the associated relaxation rate (γ) is large compared to

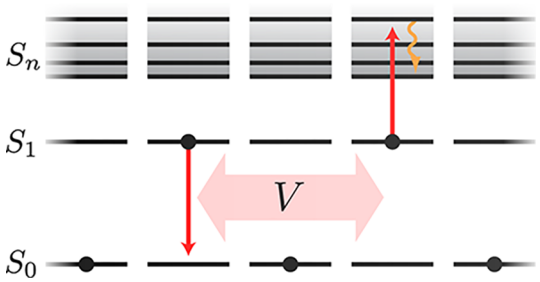

Figure 1. Microscopic representation of exciton−exciton annihilation. Coupling (V) between nearby molecules in the S_1 state lowers one molecule to the S_0 state while promoting the other to S_n (red arrows). Subsequently, phonon-assisted relaxation (yellow wiggling arrow) prohibits the regeneration of two S_1 excitations. Ultimately, the S_n excitation decays back to S_1. Hence, the overall process corresponds to the loss of one S_1 excitation.

Received: October 16, 2017
Accepted: November 30, 2017
Published: November 30, 2017

DOI: 10.1021/acs.jpclett.7b02745
J. Phys. Chem. Lett. 2017, 8, 6113−6117

the resonant coupling between molecules, the regeneration of two S_1 states is prohibited, and the overall process corresponds to the effective loss of one excitation quantum. Furthermore, EEA can then be microscopically described by Fermi's Golden Rule,

$$\Gamma = \frac{2\pi}{\hbar\gamma} \sum_{\mu,\nu} P_{\mu,\nu} \sum_{m} |\langle S_{n(m)}|H_a|\Psi_{\mu,\nu}\rangle|^2 \tag{2}$$

where the density of states (which accounts for energy conservation) is replaced by the inverse vibrational relaxation constant, $1/\gamma$.[23] $S_{n(m)}$ represents a higher-lying singlet excitation at a molecule labeled m. Delocalization of this excitation can be neglected owing to the large relaxation rate. $\Psi_{\mu,\nu}$ represents the eigenstates of the manifold of two S_1 excitations. The summation over the associated quantum numbers, μ and ν, is weighed by the Boltzmann factor $P_{\mu,\nu} = e^{-\omega_{\mu,\nu}/k_BT}/\sum_{\mu',\nu'} e^{-\omega_{\mu',\nu'}/k_BT}$, with $\omega_{\mu,\nu}$ as the eigenenergy associated with $\Psi_{\mu,\nu}$. In second quantization, the annihilation Hamiltonian appearing in eq 2 is given by

$$H_a = \sum_{m_1,m_2} V_{m_1,m_2} b^{\dagger}_{n(m_1)} b_{1(m_1)} b_{1(m_2)} + \text{H.c.} \tag{3}$$

where $b_{1(m)}$ and $b_{n(m)}$ represent the Pauli annihilation operators for S_1 and S_n excitations at molecule m, respectively, and V_{m_1,m_2} represents the resonant coupling between the $S_1 - S_n$ and $S_0 - S_1$ transitions at molecules m_1 and m_2. The double summation in eq 3 implicitly excludes $m_1 = m_2$, as will be the case for all other double summations appearing in this text.

Shown in Figure 2 are the calculated EEA rates for typical parameters representing linear J- and H-aggregates as a function

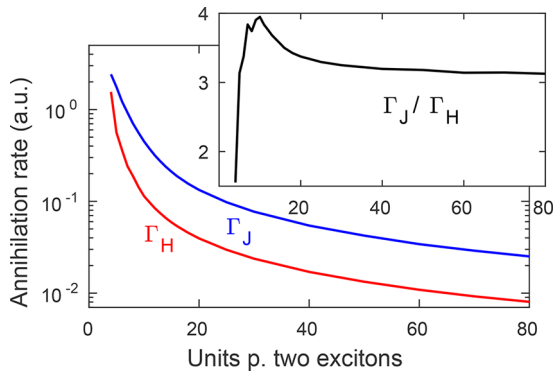

Figure 2. Annihilation rates calculated using parameters typical for (linear) J- and H-aggregates, as a function of the number of molecular units per two excitons. Inset shows the ratio between the rates. (Irregular behavior observed using less than 10 units is due to boundary effects.)

of the number of molecular units in the aggregate. Imposing periodic boundaries, such molecular chains effectively represent extended aggregates with two S_1 excitons per molecule count. The two-exciton eigenstates and -energies, $\Psi_{\mu,\nu}$ and $\omega_{\mu,\nu}$, are obtained by solving the Schrödinger equation using the Hamiltonian

$$H = \sum_{m} \epsilon_m b^{\dagger}_{1(m)} b_{1(m)} + \sum_{m_1,m_2} J_{m_1,m_2} b^{\dagger}_{1(m_1)} b_{1(m_2)} \tag{4}$$

where the first term contains the S_0–S_1 transition energies. Disorder in these energies is accounted for by drawing each ϵ_m randomly and independently from a normal distribution (centered at some m-independent value) with a standard deviation σ = 500 cm^{-1}, while sampling over 20 000 configurations. The second term accounts for dipole–dipole coupling between the S_0–S_1 transitions at molecules m_1 and m_2. Adopting the point-dipole approximation, and assuming all dipoles to be parallel, the coupling strength is given by $J_{m_1,m_2} = J_{NN}/|m_1 - m_2|^3$, using $J_{NN} = \pm$ 1000 cm^{-1}. The couplings appearing in H_a can likewise be regarded to be of dipolar form, and as such will differ from J_{m_1,m_2} mostly by a constant prefactor. Since this difference will factor out in the equations under consideration, we simply set $V_{m_1,m_2} = J_{m_1,m_2}$. Lastly, the thermal distribution $P_{\mu,\nu}$ is taken for a temperature of T = 300 K.

Figure 2 demonstrates an expected monotonous decrease of the EEA rate with increasing aggregate length, or decreasing excitation density. However, throughout, the rate for H-aggregates is found to be consistently and significantly lower than the equivalent for J-aggregates. This is particularly evident when considering the rate ratio, Γ_J/Γ_H, which rapidly converges to a value of ∼3.1. This pronounced difference is obtained by simply inverting the sign of the dipole–dipole couplings from J_{NN} = +1000 cm^{-1} (H-aggregates) to J_{NN} = −1000 cm^{-1} (J-aggregates), and suggests a fundamental principle affecting EEA that goes beyond a macroscopic representation of this process.

In order to understand the continuous difference between Γ_J and Γ_H, it is instructive to consider the limiting case of zero temperature (T = 0 K) and without disorder (σ = 0). This case can be solved analytically, yielding $\Gamma_J = 4\Gamma_H$ (assuming nearest-neighbor interactions for J_{m_1,m_2}, but point-dipole interactions for V_{m_1,m_2}, see Supporting Information). Importantly, in this case only the lowest-energy (band-bottom) eigenstate contributes to the EEA rate. The J- and H-aggregate band-bottom eigenstates are expanded in the local basis as $|\Psi_{J/H}\rangle = \sum_{m_1>m_2} c^{J/H}_{m_1,m_2}|m_1, m_2\rangle$, where $|m_1, m_2\rangle$ represents a pair of S_1 excitations at molecules m_1 and m_2. It is helpful to define symmetrized wave function coefficients as $d^{J/H}_{m_1,m_2} \equiv \Theta(m_1 - m_2)c^{J/H}_{m_1,m_2} + \Theta(m_2 - m_1)c^{J/H}_{m_2,m_1}$, where $\Theta(m)$ is the Heaviside step function (so that $d^{J/H}_{m_1,m_2} = d^{J/H}_{m_2,m_1}$). It can be shown (see Supporting Information) that under these conditions the EEA rate is given by

$$\Gamma_{J/H} = \frac{2\pi}{\hbar\gamma} \sum_{m_1} |\sum_{m_2} V_{m_1,m_2} d^{J/H}_{m_1,m_2}|^2 \tag{5}$$

Hence, the EEA rate scales as the square of the coherent sum over m_2 of the product $V_{m_1,m_2} d^{J/H}_{m_1,m_2}$. Note that this sum is independent of m_1, owing to the periodic boundaries imposed and the absence of disorder. Furthermore, the coupling V_{m_1,m_2} is monosignate and scales as $1/|m_1 - m_2|^3$, leaving the coefficients to determine the difference between J- and H-aggregates.

The symmetrized coefficients $d^{J/H}_{m_1,m_2}$ are plotted in Figure 3 for an aggregate of length 10. From this figure, the fundamental difference between J- and H-aggregates becomes evident. For J-aggregates, the coefficients are in-phase for all values of m_2. As a result, they constructively contribute to the coherent sum in eq 5. For H-aggregates, on the other hand, the coefficients are sign-alternating with m_2. This phase relation, combined with the long range of V_{m_1,m_2}, results in a destructive interference in eq 5. This behavior is akin (that is, formally similar) to super-radiance and subradiance observed upon intraband relaxation in J- and H-aggregates, respectively.[32] Similarly to this phenom-

DOI: 10.1021/acs.jpclett.7b02745
J. Phys. Chem. Lett. 2017, 8, 6113–6117

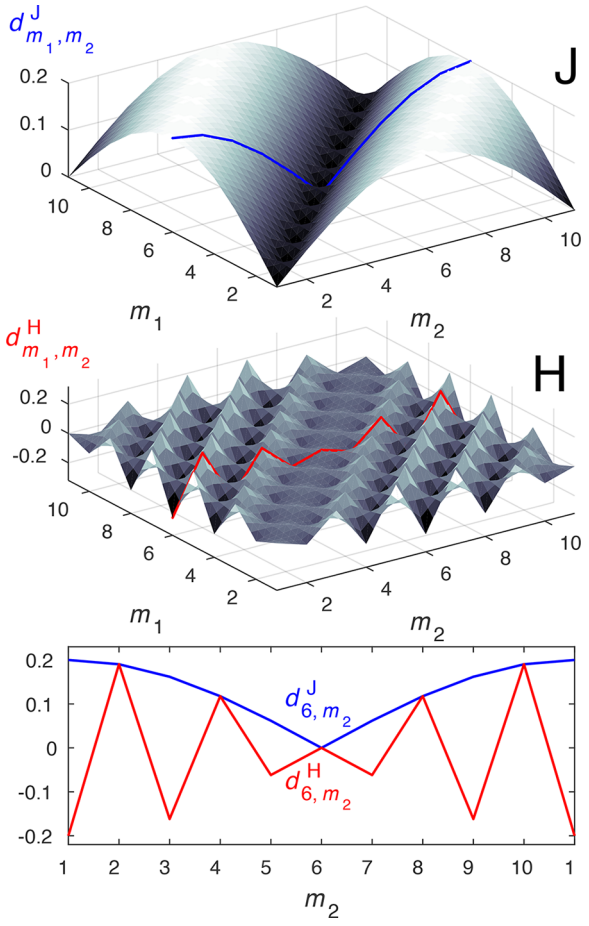

Figure 3. Symmetrized wave function coefficients of the band-bottom eigenstates of the two-exciton Hamiltonian for J- (top) and H-aggregates (middle) consisting of 10 molecules, together with a slice taken at $m_1 = 6$ (bottom).

enon, the responsible destructive interference is maximal only for the band-bottom state in the absence of disorder, but the effect is nevertheless retained when disorder is present and at finite temperatures.

Shown in Figure 4 is the ratio of Γ_J and Γ_H as a function of the disorder width (σ) and temperature (T), calculated for linear aggregates consisting of 80 molecules. Results for $\sigma = 100$ cm^{-1}, 200 cm^{-1}, 300 cm^{-1}, 400 cm^{-1}, and 500 cm^{-1} are averaged over 4000, 8000, 12 000, 16 000, and 20 000 configurations, respectively. This figure demonstrates that the contrasting behavior of J- and H-aggregates is not unique to disorder-free systems at low temperature, but applies equally well for disordered aggregates over all physically relevant temperatures. Note that with J_{m_1,m_2} taken in the point-dipole approximation, the annihilation ratio at low values of T and σ diverges with increasing aggregate length. This is in contrast to the disorder-free case at zero temperature with J_{m_1,m_2} limited to nearest-neighbors, for which the ratio asymptotically approaches 4, as shown in the Supporting Information. Although the physical origin of this difference is beyond the scope of the current work, we have performed additional calculations (not shown here) demonstrating that an extension of J_{m_1,m_2} beyond nearest neighbors yields a further suppression of annihilation for H-aggregates while yielding an enhancement for J-aggregates, which accounts for this observation. In addition, we provide in the Supporting Information calculations showing that the admixture of S_n into the band-bottom two-exciton eigenstate is strongly suppressed in H-aggregates relative to J-aggregates when V_{m_1,m_2} is treated nonperturbatively. As the irriversibility of EEA originates from the internal conversion from S_n to S_1 in this nonperturbative regime, the EEA rate is proportional to this admixture, and as such these results support the validity of our findings beyond the perturbative approach employed thus far.

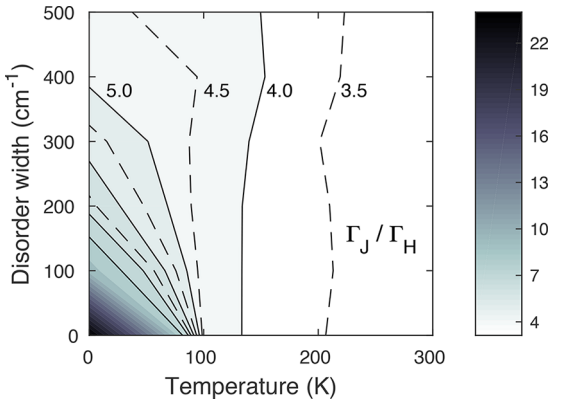

Figure 4. Ratio of the annihilation rates for J- and H-aggregates as a function of temperature and disorder width, calculated using 80 molecules per two excitons.

When separately considering the annihilation rates Γ_J and Γ_H (not shown), we observe that both experience a large increase with increasing disorder width at zero temperature, whereas at room temperature the rates are found to be fairly insensitive to disorder. We furthermore note that it would be worthwhile to extend the theory to aggregates of higher dimensionality in future work. Of particular interest is the case in which J-type behavior in one direction competes with H-type behavior in another direction,[33] which, following the findings presented here, could result in anisotropic EEA dynamics.

The above demonstration of the coherent suppression of EEA in H-aggregates adds to a recent trend connecting macroscopic material properties to the phase of quantum excitations, and its sensitivity to the sign of intermolecular couplings, through microscopic modeling. For example, recent studies have found that the interference between dipole−dipole couplings and short-ranged charge transfer interactions underlies the diversity in absorption spectra displayed by chemically near-identical molecular crystals,[34] and offers the possibility to control the exciton mobility in such materials.[35] Other studies demonstrated the importance of wave function delocalization to charge recombination at molecular heterojunctions,[36] and the crucial role of the signs of charge-transfer integrals in the suppression of this loss mechanism.[37,38] In the broader context, these studies form examples of a revived interest in coherent interference effects in molecular materials, with other prominent cases to be found in singlet exciton fission,[39] polaritons in microcavities,[40] charge currents in molecular junctions,[41] and excitation mobility in DNA.[42]

The implications of our findings to technological applications and experiments involving high excitation densities are straightforward. For molecular devices where EEA is undesirable, the selective use of H-type materials (i.e., having predominantly negative dipole−dipole couplings) is a possible means to minimize this loss mechanism. For devices where

DOI: 10.1021/acs.jpclett.7b02745
J. Phys. Chem. Lett. 2017, 8, 6113−6117

EEA serves a functional purpose, on the other hand, J-type materials are to be preferred. Our theory provides a plausible interpretation of the aforementioned experiments observing a higher EEA rate in J-aggregates compared to H-aggregates.[27,28,30,31] Generally, it predicts the contribution of EEA to nonlinear spectroscopy to be significantly smaller for H-type materials than for J-type materials. The latter has an important consequence for studies seeking to determine exciton diffusion lengths using fluence-dependent time-resolved spectroscopy, since this approach likely yields significant underestimates for H-aggregates. As such, it is of great interest to assess the accuracy of such studies through a comparison with more direct methods of determining diffusion lengths, such as optical absorption microscopy.[43,44] Drawing such a comparison will simultaneously offer a firm experimental verification of the theory proposed in this work.

In summary, we have demonstrated that the sign of dipole−dipole couplings between molecules has a profound impact on the annihilation rate between (singlet) excitons through interference of the phase relations of the two-exciton wave functions. In H-aggregates, with positive couplings, this interference is destructive as a result of which the rate is significantly suppressed. For J-aggregates, where couplings are negative, no such coherent suppression occurs. This gives rise to a factor of ∼3 difference between annihilation rates for typical J- and H-aggregates. These findings explain experimental observations, and open an avenue for the rational design of materials with desirable annihilation qualities.

■ ASSOCIATED CONTENT

Supporting Information

The Supporting Information is available free of charge on the ACS Publications website at DOI: 10.1021/acs.jpclett.7b02745.

Nonperturbative calculations, and analytical derivation of the zero-temperature exciton−exciton annihilation rates for disorder-free, periodic J- and H-aggregates (PDF)

■ AUTHOR INFORMATION

Corresponding Authors

*E-mail: r.tempelaar@gmail.com.
*E-mail: j.knoester@rug.nl.

ORCID

Roel Tempelaar: 0000-0003-0786-7304
Thomas L. C. Jansen: 0000-0001-6066-6080

Notes

The authors declare no competing financial interest.

■ ACKNOWLEDGMENTS

R.T. acknowledges The Netherlands Organisation for Scientific Research NWO for support through a Rubicon grant.

■ REFERENCES

(1) Baldo, M. A.; Holmes, R. J.; Forrest, S. R. Prospects for Electrically Pumped Organic Lasers. *Phys. Rev. B: Condens. Matter Mater. Phys.* **2002**, *66*, 035321.

(2) Akselrod, G. M.; Tischler, Y. R. R.; Young, E. R.; Nocera, D. G.; Bulovic, V. Exciton-Exciton Annihilation in Organic Polariton Microcavities. *Phys. Rev. B: Condens. Matter Mater. Phys.* **2010**, *82*, 113106.

(3) Baldo, M. A.; O'Brien, D. F.; You, Y.; Shoustikov, A.; Sibley, S.; Thompson, M. E.; Forrest, S. R. Highly Efficient Phosphorescent Emission from Organic Electroluminescent Devices. *Nature* **1998**, *395*, 151−154.

(4) Ma, Y.-Z.; Valkunas, L.; Dexheimer, S. L.; Bachilo, S. M.; Fleming, G. R. Femtosecond Spectroscopy of Optical Excitations in Single-Walled Carbon Nanotubes: Evidence for Exciton-Exciton Annihilation. *Phys. Rev. Lett.* **2005**, *94*, 157402.

(5) Nguyen, D. T.; Voisin, C.; Roussignol, P.; Roquelet, C.; Lauret, J. S.; Cassabois, G. Elastic Exciton-Exciton Scattering in Photoexcited Carbon Nanotubes. *Phys. Rev. Lett.* **2011**, *107*, 127401.

(6) Moritsubo, S.; Murai, T.; Shimada, T.; Murakami, Y.; Chiashi, S.; Maruyama, S.; Kato, Y. K. Exciton Diffusion in Air-Suspended Single-Walled Carbon Nanotubes. *Phys. Rev. Lett.* **2010**, *104*, 247402.

(7) Sun, D.; Rao, Y.; Reider, G. A.; Chen, G.; You, Y.; Brézin, L.; Harutyunyan, A. R.; Heinz, T. F. Observation of Rapid Exciton-Exciton Annihilation in Monolayer Molybdenum Disulfide. *Nano Lett.* **2014**, *14*, 5625−5629. PMID: 25171389.

(8) Nguyen, T.-Q.; Martini, I. B.; Liu, J.; Schwartz, B. J. Controlling Interchain Interactions in Conjugated Polymers: the Effects of Chain Morphology on Exciton-Exciton Annihilation and Aggregation in MEH-PPV Films. *J. Phys. Chem. B* **2000**, *104*, 237−255.

(9) Fückel, B.; Hinze, G.; Nolde, F.; Müllen, K.; Basché, T. Control of the Electronic Energy Transfer Pathway Between Two Single Fluorophores by Dual Pulse Excitation. *Phys. Rev. Lett.* **2009**, *103*, 103003.

(10) Gélinas, S.; Kirkpatrick, J.; Howard, I. A.; Johnson, K.; Wilson, M. W. B.; Pace, G.; Friend, R. H.; Silva, C. Recombination Dynamics of Charge Pairs in a Push-Pull Polyfluorene-Derivative. *J. Phys. Chem. B* **2013**, *117*, 4649−4653. PMID: 23151039.

(11) Valkunas, L.; van Stokkum, I. H.; Berera, R.; van Grondelle, R. Exciton Migration and Fluorescence Quenching in LHCII Aggregates: Target Analysis Using a Simple Nonlinear Annihilation Scheme. *Chem. Phys.* **2009**, *357*, 17−20. Excited State Dynamics in Light Harvesting Materials.

(12) Brüggemann, B.; Christensson, N.; Pullerits, T. Temperature Dependent Exciton-Exciton Annihilation in the LH2 Antenna Complex. *Chem. Phys.* **2009**, *357*, 140−143. Excited State Dynamics in Light Harvesting Materials.

(13) Müller, M. G.; Lambrev, P.; Reus, M.; Wientjes, E.; Croce, R.; Holzwarth, A. R. Singlet Energy Dissipation in the Photosystem II Light-Harvesting Complex Does Not Involve Energy Transfer to Carotenoids. *ChemPhysChem* **2010**, *11*, 1289−1296.

(14) Den Hollander, W. T. F.; Bakker, J.; VanGrondelle, R. Trapping, Loss and Annihilation of Excitations in a Photosynthetic System. I. Theoretical Aspects. *Biochim. Biophys. Acta, Bioenerg.* **1983**, *725*, 492−507.

(15) Fennel, F.; Lochbrunner, S. Exciton-Exciton Annihilation in a Disordered Molecular System by Direct and Multistep Förster Transfer. *Phys. Rev. B: Condens. Matter Mater. Phys.* **2015**, *92*, 140301.

(16) Barzda, V.; Gulbinas, V.; Kananavicius, R.; Cervinskas, V.; van Amerongen, H.; van Grondelle, R.; Valkunas, L. Singlet−Singlet Annihilation Kinetics in Aggregates and Trimers of LHCII. *Biophys. J.* **2001**, *80*, 2409−2421.

(17) Shaw, P. E.; Ruseckas, A.; Peet, J.; Bazan, G. C.; Samuel, I. D. W. Exciton-Exciton Annihilation in Mixed-Phase Polyfluorene Films. *Adv. Funct. Mater.* **2010**, *20*, 155−161.

(18) Cook, S.; Liyuan, H.; Furube, A.; Katoh, R. Singlet Annihilation in Films of Regioregular Poly(3-Hexylthiophene): Estimates for Singlet Diffusion Lengths and the Correlation Between Singlet Annihilation Rates and Spectral Relaxation. *J. Phys. Chem. C* **2010**, *114*, 10962−10968.

(19) Marciniak, H.; Li, X.-Q.; Würthner, F.; Lochbrunner, S. One-Dimensional Exciton Diffusion in Perylene Bisimide Aggregates. *J. Phys. Chem. A* **2011**, *115*, 648−654. PMID: 21192672.

(20) Tamai, Y.; Matsuura, Y.; Ohkita, H.; Benten, H.; Ito, S. One-Dimensional Singlet Exciton Diffusion in Poly(3-Hexylthiophene) Crystalline Domains. *J. Phys. Chem. Lett.* **2014**, *5*, 399−403.

(21) Lin, J. D. A.; Mikhnenko, O. V.; Chen, J.; Masri, Z.; Ruseckas, A.; Mikhailovsky, A.; Raab, R. P.; Liu, J.; Blom, P. W. M.; Loi, M. A.; et al. Systematic Study of Exciton Diffusion Length in Organic

DOI: 10.1021/acs.jpclett.7b02745
J. Phys. Chem. Lett. 2017, 8, 6113−6117

Semiconductors by Six Experimental Methods. *Mater. Horiz.* **2014**, *1*, 280−285.
(22) Malyshev, V.; Glaeske, H.; Feller, K.-H. Exciton-Exciton Annihilation in Linear Molecular Aggregates at Low Temperature. *Chem. Phys. Lett.* **1999**, *305*, 117−122.
(23) Ryzhov, I. V.; Kozlov, G. G.; Malyshev, V. A.; Knoester, J. Low-Temperature Kinetics of Exciton−Exciton Annihilation of Weakly Localized One-Dimensional Frenkel Excitons. *J. Chem. Phys.* **2001**, *114*, 5322−5329.
(24) Brüggemann, B.; Herek, J. L.; Sundström, V.; Pullerits, T.; May, V. Microscopic Theory of Exciton Annihilation: Application to the LH2 Antenna System. *J. Phys. Chem. B* **2001**, *105*, 11391−11394.
(25) May, V. Kinetic Theory of Exciton−Exciton Annihilation. *J. Chem. Phys.* **2014**, *140*, 054103.
(26) Hader, K.; May, V.; Lambert, C.; Engel, V. Identification of Effective Exciton-Exciton Annihilation in Squaraine-Squaraine Co-polymers. *Phys. Chem. Chem. Phys.* **2016**, *18*, 13368−13374.
(27) Khairutdinov, R. F.; Serpone, N. Photophysics of Cyanine Dyes: Subnanosecond Relaxation Dynamics in Monomers, Dimers, and H- and J-Aggregates in Solution. *J. Phys. Chem. B* **1997**, *101*, 2602−2610.
(28) Scheblykin, I. G.; Sliusarenko, O. Y.; Lepnev, L. S.; Vitukhnovsky, A. G.; Van der Auweraer, M. Strong Nonmonotonous Temperature Dependence of Exciton Migration Rate in J Aggregates at Temperatures from 5 to 300 K. *J. Phys. Chem. B* **2000**, *104*, 10949−10951.
(29) King, S. M.; Dai, D.; Rothe, C.; Monkman, A. P. Exciton Annihilation in a Polyfluorene: Low Threshold for Singlet-Singlet Annihilation and the Absence of Singlet-Triplet Annihilation. *Phys. Rev. B: Condens. Matter Mater. Phys.* **2007**, *76*, 085204.
(30) Ito, F.; Inoue, T.; Tomita, D.; Nagamura, T. Excited-State Relaxation Process of Free-Base and Oxovanadium Naphthalocyanine in Near-Infrared Region. *J. Phys. Chem. B* **2009**, *113*, 5458−5463.
(31) Völker, S. F.; Schmiedel, A.; Holzapfel, M.; Renziehausen, K.; Engel, V.; Lambert, C. Singlet-Singlet Exciton Annihilation in an Exciton-Coupled Squaraine-Squaraine Copolymer: A Model Toward Hetero-J-Aggregates. *J. Phys. Chem. C* **2014**, *118*, 17467−17482.
(32) Spano, F. C. The Spectral Signatures of Frenkel Polarons in H- and J-Aggregates. *Acc. Chem. Res.* **2010**, *43*, 429−439. PMID: 20014774.
(33) Yamagata, H.; Spano, F. C. Interplay Between Intrachain and Interchain Interactions in Semiconducting Polymer Assemblies: The HJ-Aggregate Model. *J. Chem. Phys.* **2012**, *136*, 184901.
(34) Yamagata, H.; Maxwell, D. S.; Fan, J.; Kittilstved, K. R.; Briseno, A. L.; Barnes, M. D.; Spano, F. C. HJ-Aggregate Behavior of Crystalline 7,8,15,16-Tetraazaterrylene: Introducing a New Design Paradigm for Organic Materials. *J. Phys. Chem. C* **2014**, *118*, 28842−28854.
(35) Hestand, N. J.; Tempelaar, R.; Knoester, J.; Jansen, T. L. C.; Spano, F. C. Exciton Mobility Control Through sub−Å Packing Modifications in Molecular Crystals. *Phys. Rev. B: Condens. Matter Mater. Phys.* **2015**, *91*, 195315.
(36) Bittner, E. R.; Lankevich, V.; Gelinas, S.; Rao, A.; Ginger, D. A.; Friend, R. H. How Disorder Controls the Kinetics of Triplet Charge Recombination in Semiconducting Organic Polymer Photovoltaics. *Phys. Chem. Chem. Phys.* **2014**, *16*, 20321−20328.
(37) Tempelaar, R.; Koster, L. J. A.; Havenith, R. W. A.; Knoester, J.; Jansen, T. L. C. Charge Recombination Suppressed by Destructive Quantum Interference in Heterojunction Materials. *J. Phys. Chem. Lett.* **2016**, *7*, 198−203. PMID: 26683652.
(38) Tempelaar, R.; Koster, L. J. A.; Havenith, R. W. A.; Knoester, J.; Jansen, T. L. C. Correction to "Charge Recombination Suppressed by Destructive Quantum Interference in Heterojunction Materials. *J. Phys. Chem. Lett.* **2016**, *7*, 3659−3659. PMID: 27598409.
(39) Petelenz, P.; Snamina, M. Locally Broken Crystal Symmetry Facilitates Singlet Exciton Fission. *J. Phys. Chem. Lett.* **2016**, *7*, 1913−1916. PMID: 27152577.
(40) Herrera, F.; Spano, F. C. Dark Vibronic Polaritons and the Spectroscopy of Organic Microcavities. *Phys. Rev. Lett.* **2017**, *118*, 223601.
(41) Solomon, G. C.; Herrmann, C.; Hansen, T.; Mujica, V.; Ratner, M. A. Exploring Local Currents in Molecular Junctions. *Nat. Chem.* **2010**, *2*, 223−228.
(42) Liu, C.; Xiang, L.; Zhang, Y.; Zhang, P.; Beratan, D. N.; Li, Y.; Tao, N. Engineering Nanometre-Scale Coherence in Soft Matter. *Nat. Chem.* **2016**, *8*, 941−945.
(43) Devadas, M. S.; Devkota, T.; Johns, P.; Li, Z.; Lo, S. S.; Yu, K.; Huang, L.; Hartland, G. V. Imaging Nano-Objects by Linear and Nonlinear Optical Absorption Microscopies. *Nanotechnology* **2015**, *26*, 354001.
(44) Wan, Y.; Stradomska, A.; Knoester, J.; Huang, L. Direct Imaging of Exciton Transport in Tubular Porphyrin Aggregates by Ultrafast Microscopy. *J. Am. Chem. Soc.* **2017**, *139*, 7287−7293. PMID: 28480703.

DOI: 10.1021/acs.jpclett.7b02745
J. Phys. Chem. Lett. 2017, 8, 6113−6117